PLAXIS Version 8
Validation Manual

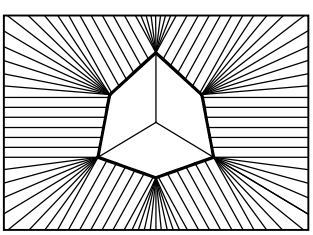

TABLE OF CONTENTS

1 INTRODUCTION

The performance and accuracy of PLAXIS has been carefully tested by carrying out analyses of problems with known analytical solutions. A selection of these benchmark analyses is described in Chapters 2 to 4. PLAXIS has also been used to carry out predictions and back-analysis calculations of the performance of full-scale structures as additional checks on performance and accuracy.

Elastic benchmark problems: A large number of elasticity problems with known exact solutions is available for use as benchmark problems. A selection of elastic calculations is described in Chapter 2; these particular analyses have been selected because they resemble the calculations that PLAXIS might be used for in practice.

Plastic benchmark problems: A series of benchmark calculations involving plastic material behaviour is described in Chapter 3. This series includes the calculation of collapse loads and the analysis of slip at an interface. As for the elastic benchmarks only problems with known exact solutions are considered.

Groundwater flow and consolidation: A series of groundwater flow benchmark calculations have been carried out to validate this type of calculations; these benchmarks are described in the Chapter 4. This chapter also contains some verification examples of Consolidation analysis.

Case studies: PLAXIS has been used extensively for the prediction and back-analysis of full scale projects. This type of calculations may be used as a further check on the performance of PLAXIS provided that good quality soil data and measurements of structural performance are available. Some such projects are published in the PLAXIS Bulletin and on the internet site: http://www.plaxis.nl. Other validation examples and comparisons with measured data, particular on the application of advanced soil models, can be found in Chapter 8 of the Material Models Manual.

2 ELASTICITY PROBLEMS WITH KNOWN THEORETICAL SOLUTIONS

A series of elastic benchmark calculations is described in this Chapter. In each case the analytical solutions may be found in many of the various textbooks on elasticity solutions, for example Giroud (1972) and Poulos & Davis (1974).

2.1 SMOOTH RIGID STRIP FOOTING ON ELASTIC SOIL

Input: The problem of a smooth strip footing on an elastic soil layer with depth *H* is shown in Figure 2.1. This figure also shows relevant soil data and the finite element mesh used in the calculation. 15-node soil elements are employed. A uniform vertical displacement of 10 mm is prescribed to the footing and the indentation force, *F*, is calculated from the results of the finite element calculation. Since the problem is symmetric it is possible to model only one half of the situation as shown in Figure 2.1.

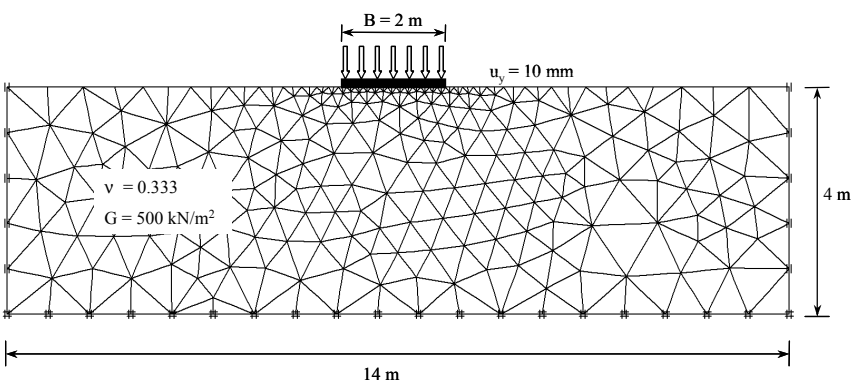

Figure 2.1 Problem geometry

Output: The scaled deformation of the finite element mesh at the end of the elastic analysis is shown in Figure 2.2. The footing force resulting from a rigid indentation of 10 mm is calculated to be *F*=15.24 kN.

$$\text{Settlement} = \frac{F\delta}{2(1+\nu)G} \quad \text{with} \quad \delta = 0.88 \quad \text{for} \quad \frac{H}{\frac{1}{2}B} = 4$$

Verification: Giroud (1972) gives the analytical solution to this problem in the formula above, where *H* is the depth of the layer, *B* is the total width of the footing and δ is a constant. For the dimensions and material properties used in the finite element analysis this solution gives a footing force of 15.15 kN. The error in the numerical solution is therefore about 0.6%.

Figure 2.3 gives both the analytical and numerical results for the pressure distribution underneath the footing. This figure shows that the numerical results agree very well with the analytical solution.

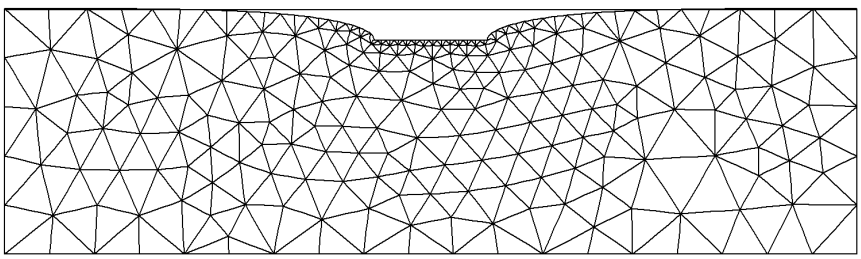

Figure 2.2 Deformed mesh

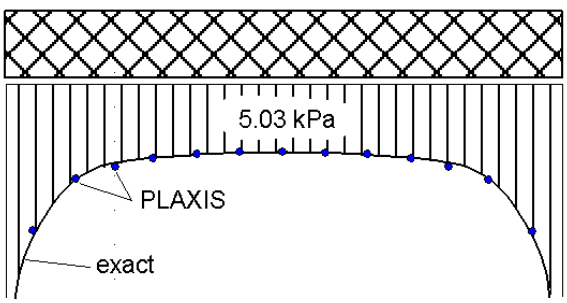

Figure 2.3 Pressure distribution at footing

2.2 STRIP LOAD ON ELASTIC GIBSON SOIL

Input: Figure 2.4 shows the mesh and the soil data for a plane strain calculation of the settlement of a strip load on Gibson soil. (Gibson soil is an elastic layer in which the shear modulus increases linearly with depth). Using z to denote depth, the shear modulus, G, used in the calculation is given by: $G = \alpha z = 100.z$. With a Poisson's ratio of 0.495, the Young's modulus varies by: $E = 299\ z$. In order to prescribe this variation of Young's modulus in the material properties window the reference value of Young's modulus, E_{ref}, is taken very small and the *Advanced* option is selected from the *Parameters* tab sheet . The increase of Young's modulus $E_{increment}$ is set to 299 and the reference level y_{ref} is entered as 4.0 m, being the top of the geometry.

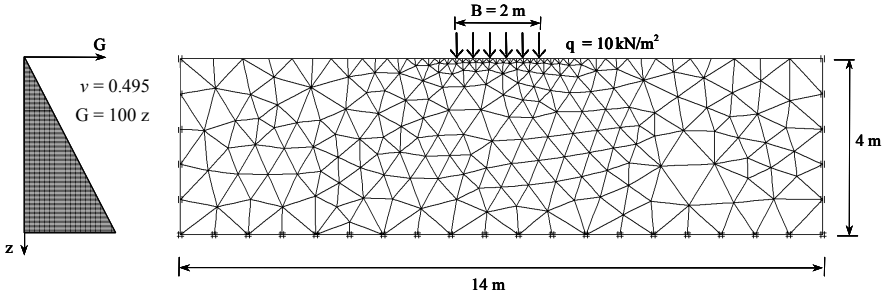

Figure 2.4 Problem geometry

Output: An exact solution to this problem is only available for the case of a Poisson's ratio of 0.5; in the PLAXIS calculation a value of 0.495 is used for the Poisson's ratio in order to approximate this incompressibility condition. The numerical results show an almost uniform settlement of the soil surface underneath the strip load as can be seen from the velocity contour plot in Figure 2.5. The computed settlement is 0.047 m at the centre of the strip load.

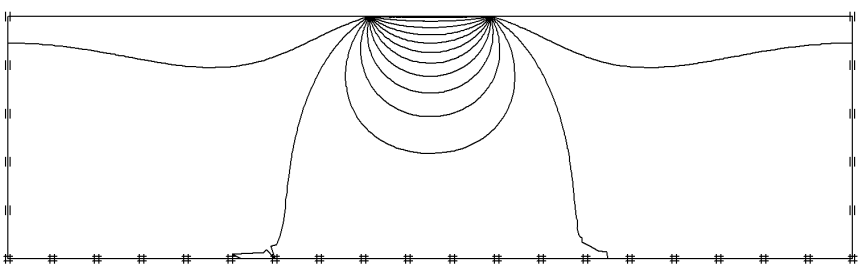

Figure 2.5 Vertical displacement contours

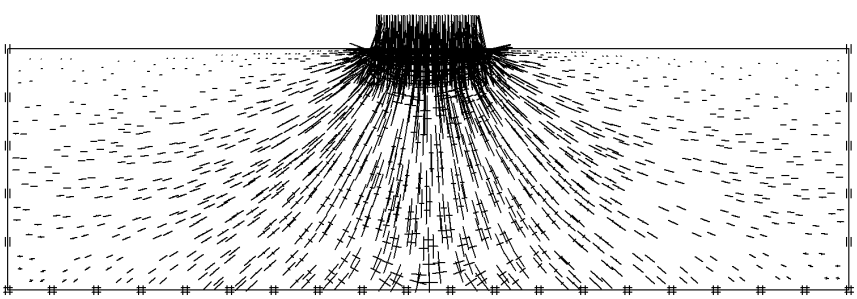

Figure 2.6 Total stresses in soil

Verification: The analytic solution is exact only for an infinite half-space, whereas the PLAXIS solution is obtained for a layer of finite depth. However, the effect of a shear modulus that increases linearly with depth is to localise the deformations near the surface; it would therefore be expected that the finite thickness of the layer will only have a small effect on the results. The exact solution for this particular problem, as given by Gibson (1967), gives a uniform settlement beneath the load of magnitude:

$$\text{Settlement} = \frac{q}{2\ \alpha}$$

In this case the exact solution gives a settlement of 0.05 m. The numerical solution is 6% lower than the exact solution.

2.3 BENDING OF BEAMS

Input: For the verification of plates (beams) two problems are considered. These problems involve a single point load and a uniformly distributed load on a beam respectively, as indicated in Figure 2.7. For these problems the characteristics of a HEB 200 steel beam have been adopted. In a plane strain model, the beam is in fact a plate of 1 m width in the out of plane direction. The properties, the dimensions and the load of the beam are:

$EA = 1.64 \cdot 10^6$ kN	$EI = 1200$ kNm^2	$\nu = 0.0$
$l = 2$ m	$F = 100$ kN	$q = 100$ kN/m

Beams cannot be used individually. A single block cluster may be used to create the geometry. The two beams are added to the bottom line with a spacing in between. Use point fixities on the end points of the beam. A very coarse mesh is sufficient to model the situation. In the *Initial conditions* mode the soil cluster can be deactivated so that only the beams remain.

Figure 2.7 Loading scheme for testing beams

Output: The results of the two calculations are plotted in Figure 2.8, Figure 2.9 and Figure 2.10. For the extreme moments and displacements we find:

Point load:	$M_{max} = 50.0$ kNm	$u_{max} = 13.96$ mm
Distributed load:	$M_{max} = 50.0$ kNm	$u_{max} = 17.43$ mm

Figure 2.8 Computed distribution of moments

Figure 2.9 Shear forces

Figure 2.10 Computed displacements

Verification: As a first verification, it is observed from Figure 2.8a and Figure 2.8b that PLAXIS yields the correct distribution of moments. For further verification we consider the well-know formulas as listed below. These formulas give approximately the values as obtained from the PLAXIS analysis.

Point load:	$M_{\max} = \frac{1}{4} Fl = 50\,\text{kNm}$	$u_{\max} = \frac{1}{48}\frac{F\,l^3}{EI} = 13.89\,\text{mm}$
Distributed load:	$M_{\max} = \frac{1}{8} ql^2 = 50\,\text{kNm}$	$u_{max} = \frac{5}{384}\frac{q\,l^4}{EI} = 17.36\,\text{mm}$

2.4 BENDING OF PLATES

Input: In an axisymmetric analysis, plates may be used as circular plates. The latter two verification examples involve a uniformly distributed load q on a circular plate. In one example the plate can rotate freely at the boundary and in the other example the plate is clamped, as indicated in Figure 2.11.

Solution: For the situation of a circular plate with a uniformly distributed load one can elaborate and solve a differential equation. The analytical solutions for this equation depend on the boundary conditions. For the plate with free rotation at the boundary one finds:

Settlement:

$$w = \frac{q\,R^4}{64D}\left(\frac{5+\nu}{1+\nu} - \frac{6+2\nu}{1+\nu}\frac{r^2}{R^2} + \frac{r^4}{R^4}\right) \qquad D = \frac{EI_{plaxis}}{1-\nu^2}$$

Moments:

$$m_{rr} = \frac{q\,R^2}{16}\left((3+\nu) - (3+\nu)\frac{r^2}{R^2}\right) \qquad m_{tt} = \frac{q\,R^2}{16}\left((3+\nu) - (1+3\nu)\frac{r^2}{R^2}\right)$$

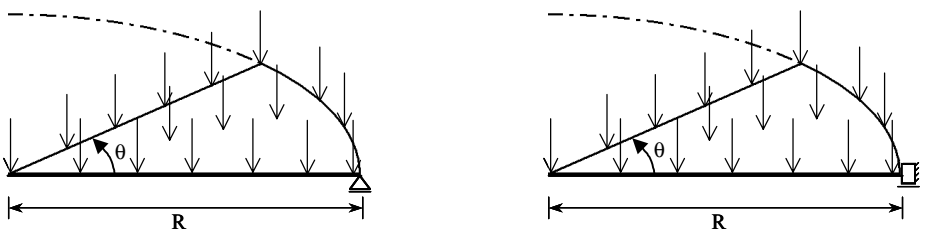

Figure 2.11 Loading scheme for testing axisymmetric plates

Using R = 1 m, d = 0.1 m, q = 1 kN/m^2, ν = 0 and EI = 1 kNm^2/m, this gives:

In the centre:	w = 0.078125m	Numerical:	w = 0.078625 m
(r = 0)	m_{rr} = 0.18750 kNm/m	Numerical:	m_{rr} = 0.18630 kNm/m
At $r = R/2$:	w = 0.055664 m	Numerical:	w = 0.056039 m
	m_{rr} = 0.140625 kNm/m	Numerical:	m_{rr} = 0.140625 kNm/m

For the plate with a clamped boundary one finds:

Settlement:

$$w = \frac{q\,R^4}{64D}\left(1 - \frac{r^2}{R^2}\right)^2$$

Moments:

$$m_{rr} = \frac{q\,R^2}{16}\left((1+\nu) - (3+\nu)\frac{r^2}{R^2}\right) \qquad m_{tt} = \frac{q\,R^2}{16}\left((1+\nu) - (1+3\nu)\frac{r^2}{R^2}\right)$$

Using R = 1 m, d = 0.1 m, q = 1 kN/m^2, ν = 0 and EI = 1 kNm^2/m, this gives:

In the centre:	w = 0.01563 m	Numerical:	w = 0.016125 m
(r = 0)	m_{rr} = 0.06250 kNm/m	Numerical:	m_{rr} = 0.06263 kNm/m
At r = R/2:	w = 0.008789 m	Numerical:	w = 0.009164 m
	m_{rr} = 0.015625 kNm/m	Numerical:	m_{rr} = 0.015625 kNm/m
At r = R:	m_{rr} = -0.125 kNm/m	Numerical:	m_{rr} = -0.125 kNm/m

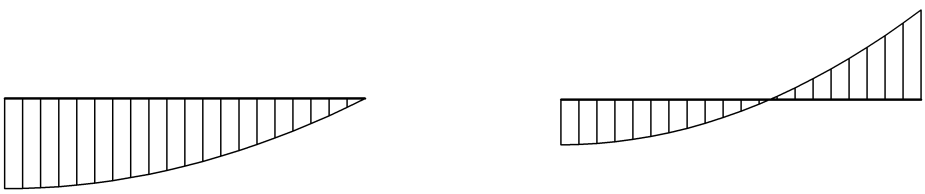

Figure 2.12 Computed distribution of moments

Figure 2.13 Computed displacements

Verification: The settlement difference is mainly due to shear deformation, which is included in the numerical solution but not in the analytical solution. Apart from this, the numerical results are very close to the analytical solution.

2.5 PERFORMANCE OF SHELL ELEMENTS

A beam in PLAXIS can be applied as a tunnel lining. By using this element, 3 types of deformations are taken into account: shear deformation, compression due to normal forces and obviously bending.

Input: A ring with a radius of R=5 m is considered. The Young's modulus and the Poisson's ratio of the material are taken respectively as E=10^6 kPa and ν=0. For the thickness of the ring cross section, H, several different values are taken so that we have rings ranging from very thin to very thick. In order to model such a ring the bottom point of the ring is fixed with respect to translation and the top point is allowed to move only in the vertical direction. Then the load F=0.2 kN/m is applied only at the top point. Geometric non-linearity is not taken into account.

Output: The calculated vertical deflections at the top point are presented in Figure 2.14. The deformed shape of the ring is also shown in Figure 2.14. The calculated normal force at the belly of the ring is 0.50 for all different values of ring thickness. The calculated bending moment at the belly varies from 0.182 to 0.189 as the ring changes from thin to thick. Typical graphs of the bending moment and normal force are shown in Figure 2.15a and Figure 2.15b.

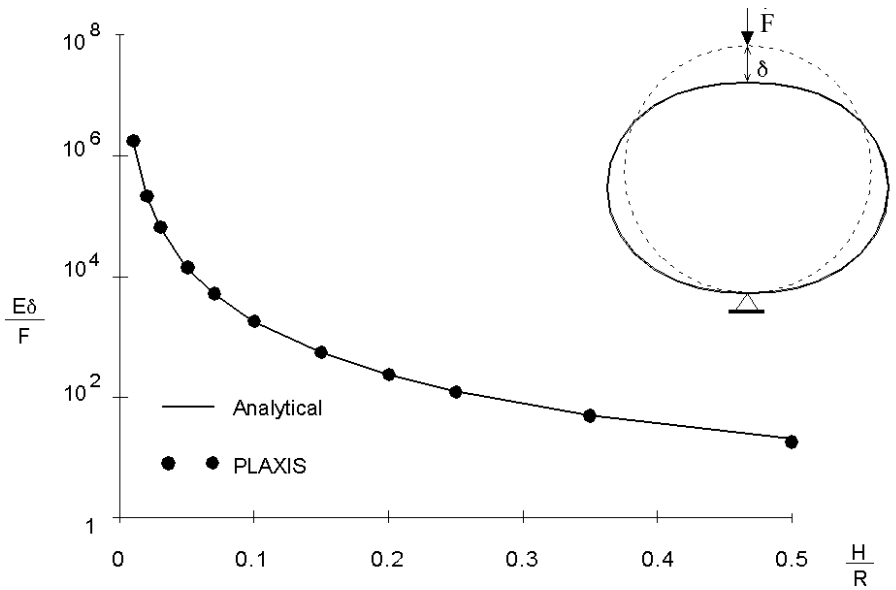

Figure 2.14 Calculated deflections compared with analytical solutions

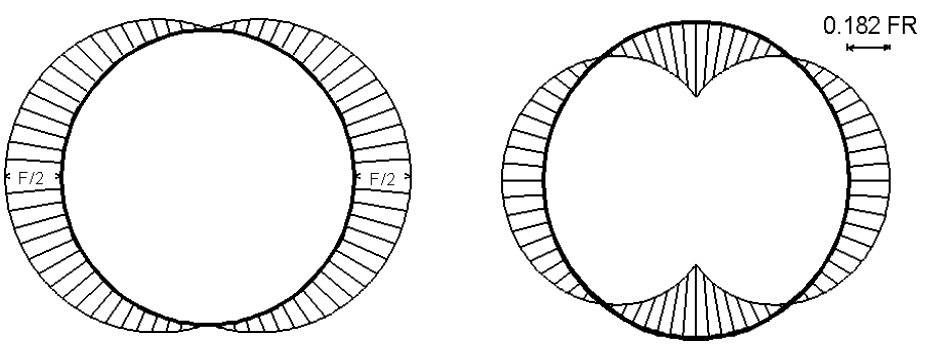

(a) (b)

Figure 2.15 Normal forces (a) and Bending moments (b)

Verification: The analytical solution for the deflection of the ring is given by Blake (1959), and the analytical solution for the bending moment and the normal force can be found from Roark (1965). The vertical displacement at the top of the ring is given by the following formula:

$$\delta = \frac{F\lambda}{E}\left[1.788\lambda^2 + 3.091\frac{0.637}{1+12\lambda^2}\right] \quad \text{with} \quad \lambda = \frac{R}{H}$$

The solid curve in Figure 2.14 is plotted according to this formula. It can be seen that the deflections calculated by PLAXIS fit the theoretical solutions very well. Only for a very thick ring some errors are observed, which is about 8% for *H/R*=0.5. But for thin rings the error is nearly zero. The analytical solution for the bending moment and normal force at the belly is 0.182 and 0.5 respectively. Thus even for very thick rings the error in the bending moment is just 4%, and the error in the normal force is only 0.2%.

2.6 UPDATED MESH ANALYSIS OF A CANTILEVER

The range of problems with known solutions involving large displacement effects that may be used to test the large displacement options in PLAXIS is very limited. The large displacement elastic bending of a cantilever beam, however, is one problem which is well suited as a large displacement benchmark problem since a known analytical solution exists, Mattiasson (1981).

Geometry non-linearity is of major importance in problems involving slender structural members like beams, plates and shells. Indeed, phenomena like buckling and bulging cannot be described without considering geometry changes. Soil bodies, however, are far from slender and consequently, most finite element formulations tacitly disregard changes in geometry. This also applies to conventional PLAXIS calculations. Users should check such results by considering the truly deformed mesh. In most practical cases this will indicate very little change of geometry. In some particular cases, however, it may be significant.

For special problems of extreme large deformation an *Updated mesh analysis* is needed. For this reason PLAXIS involves a special module. For details on the implementation the reader is referred the PhD thesis by Van Langen (1991). This module was programmed using the *Updated Lagrangian formulation* as described by McMeeking and Rice (1975).

Analysis: The analysis relates to the calculation of the horizontal and vertical tip displacement for the cantilever beam shown in Figure 2.16. Two meshes are used in the PLAXIS analysis: One composed of triangular (soil) elements with a thickness of 0.01 m and one composed of beam elements with zero thickness.

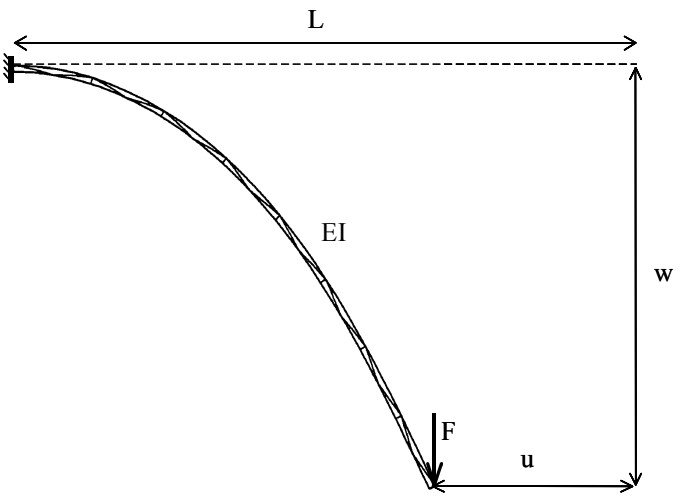

Figure 2.16 True deformation of elastic cantilever

Results: The computed load-displacement curves are plotted in Figure 2.18. The numerical results of both the soil elements and the beam elements are clearly in close agreement with the analytical solution.

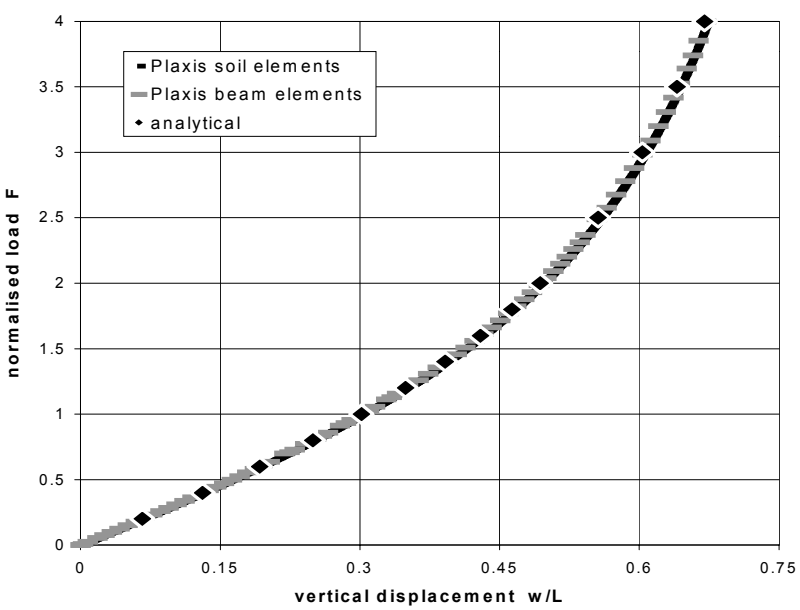

Figure 2.17 Significant geometric non-linearity

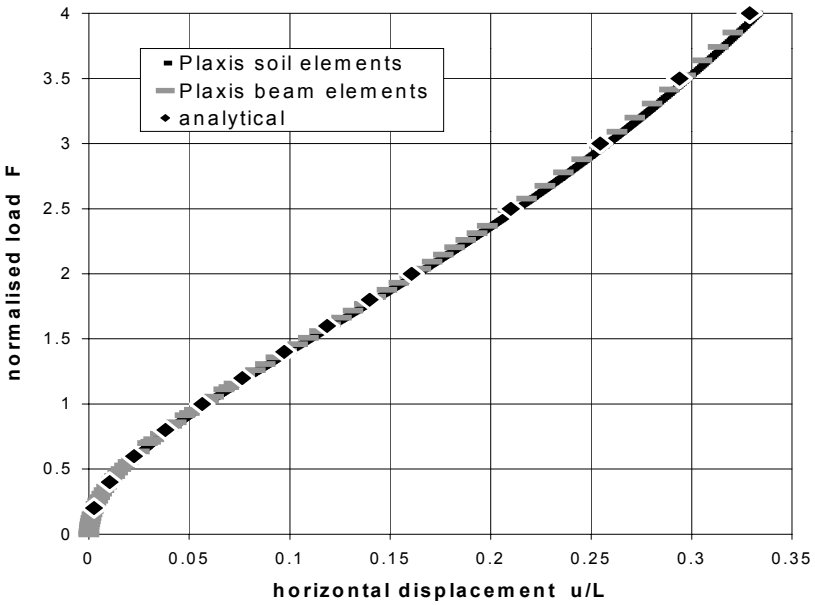

Figure 2.18 Numerical results agree with theory

3 PLASTICITY PROBLEMS WITH THEORETICAL COLLAPSE LOADS

In this Chapter, two footing collapse problems involving plastic material behaviour are presented. The first involves a smooth circular footing on a frictional soil and the second involves a strip footing on a cohesive soil with strength increasing linearly with depth. Also, an interface plasticity problem and a cylindrical cavity expansion problem are discussed.

3.1 BEARING CAPACITY OF CIRCULAR FOOTING

Input: Figure 3.1 shows the mesh and material data for a smooth rigid circular footing with radius R=1m on a frictional soil. The thickness of the soil layer is taken 4 metres and the material behaviour is represented by the Mohr-Coulomb model. The analysis is carried out using an axisymmetric model. This is a typical situation where the 15-noded elements are preferable, since lower order elements will over-predict the failure load. The initial stresses are generated by means of the K_0-procedure using a K_0-value of 0.5. During the Plastic calculation, Staged construction, the *Prescribed displacements* are increased until failure. Note that for an axisymmetric PLAXIS calculation, the mesh represents a wedge of an included angle θ of one radian; the calculated reaction must therefore be multiplied by 2π to obtain the load corresponding to a full circular footing.

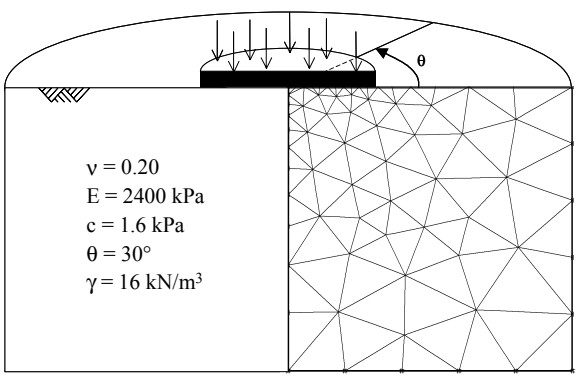

Figure 3.1 Problem geometry

Output: The load-displacement curve for the footing is shown in Figure 3.2. The calculated collapse load is 110 kN/rad, which corresponds to an average vertical stress at failure, p_{max} with:

$$p_{\max} = \frac{110 \times 2\pi}{\pi R^2} = 220\,\text{kPa}$$

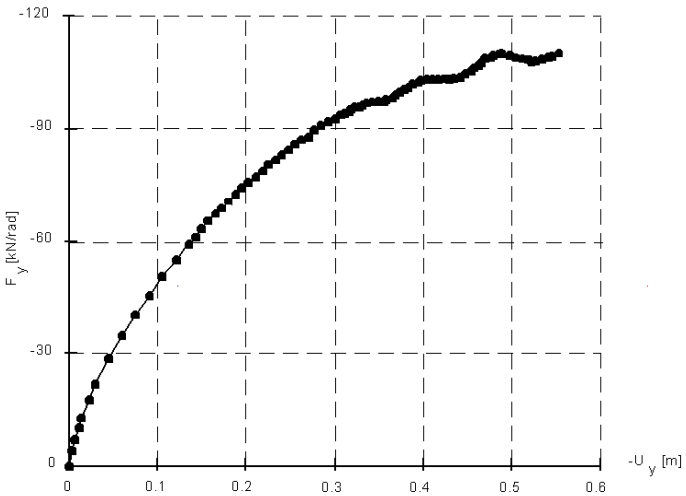

Figure 3.2 Load displacement curve

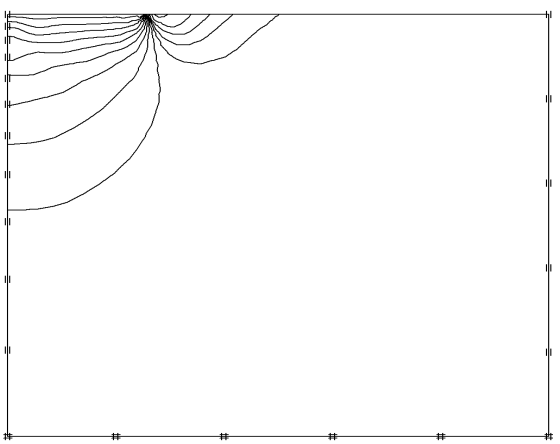

Figure 3.3 Vertical displacement contours at failure

Verification: The exact solution for the collapse load problem is derived by Cox (1962) for $\gamma R/c = 10$ and $\phi = 30°$. The solution reads:

$$p_{max} = 141 \times c = 141 \times 1.6 = 225.6 \text{ kPa}$$

The relative error of the result calculated with PLAXIS remains within 2.5%.

3.2 BEARING CAPACITY OF STRIP FOOTING

Problem: In practice it is often found that clay type soils have a strength that increases with depth. The influence of this type of strength variation is particularly important for foundations with large physical dimensions. A series of plastic collapse solutions for rigid plane strain footings on soils with strength increasing linearly with depth has been derived by Davis and Booker (1973). Some of these solutions are used to verify the performance of PLAXIS for this class of problems.

Input: The dimensions and material properties of the structure are shown in Figure 3.4. Because of symmetry, only half of the geometry is modelled using 15 node elements. The cohesion at the soil surface, c_{ref}, is taken 1 kN/m^2. In the Advanced settings, the cohesion gradient, $c_{increment}$, is set equal to 2 kN/m^2/m, using a reference level, y_{ref} = 2 m (= top of layer). The stiffness at the top is given by E_{ref} = 299 kN/m^2 and the increase of stiffness with depth is defined by $E_{increment}$ = 498 kN/m^2/m. Calculations are carried out for a rough and a smooth footing.

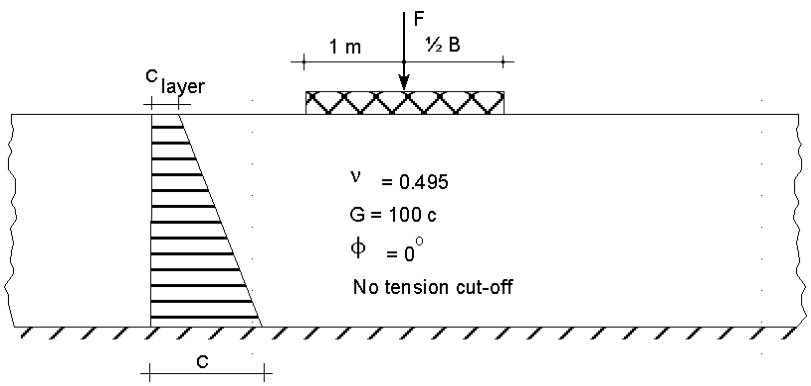

Figure 3.4 Problem geometry

Output: The calculated maximum average vertical stress under the smooth footing is 7.86 kN/m^2, giving a bearing capacity of 15.72 kN/m. For the rough footing this is 9.25 kN/m^2, giving a bearing capacity of 18.5 kN/m. The computed load-displacement curves are shown in Figure 3.6.

Verification: The analytical solution derived by Davis & Booker (1973) for the mean ultimate vertical stress beneath the footing, p_{max} , is:

$$p_{\max} = \frac{F}{B} = \beta \left[(2+\pi) c_{layer} + \frac{B \times c_{depth}}{4} \right]$$

where B is the footing width and β is a factor that depends on the footing roughness and the rate of increase of clay strength with depth. The appropriate values of β in this case

are 1.27 for the smooth footing and 1.48 for the rough footing. The analytical solution therefore gives average vertical stresses at collapse of 7.8 kN/m^2 for the smooth footing and 9.1 kN/m^2 for the rough footing. These results indicate that the errors in the PLAXIS solution are 0.77% and 1.6% respectively.

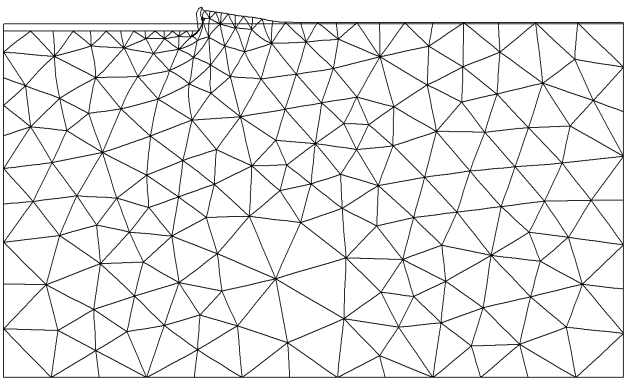

Figure 3.5 Deformed mesh (smooth)

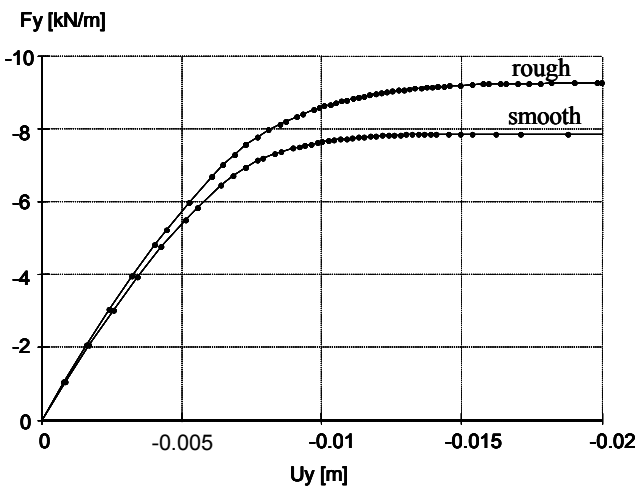

Figure 3.6 Load displacement curves

3.3 SLIDING BLOCK FOR TESTING INTERFACES

Input: One of the particular features of PLAXIS is the use of interfaces for modelling soil-structure interaction. In this section the performance of these elements is verified by means of a sliding block as shown in Figure 3.7. The properties of this concrete block are listed below.

The mesh is shown in Figure 3.8. A local refinement was used at the lower right-hand geometry point, since stress concentrations are to be expected there. An interface is used to model the sliding at the base of the block. The block is modelled as a stiff linear elastic material. The properties of the interface are stored in a separate elastoplastic data set. The adhesion is small so that sliding is dominated by friction.

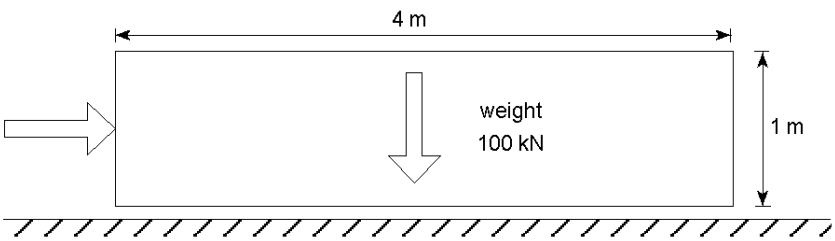

Figure 3.7 Sliding block

At the left side, a prescribed horizontal displacement of 0.1 m is applied, but the nodes at this side are free to move vertically. Bottom nodes are fully fixed. All other nodes are entirely free. The self weight stresses (γ=25 kN/m^3) are switched on using K_0=0.

Block properties:

Linear elastic E=30 GN/m^2 ν=0.0

Interface properties:

Mohr-Coulomb E=3.0 GN/m^2 ν=0.45 ϕ_w=26.6° c_w=2.5 kN/m^2

Output: On pushing the block to the right, it hardly deforms. PLAXIS gives an internal stress distribution as shown in Figure 3.9. The interface elements show that the contact stresses are largest at the right hand side. This is plausible as the pushing introduces a rotation moment.

Besides graphical output, PLAXIS gives values for the horizontal force. The failure force is 60.4 kN/m.

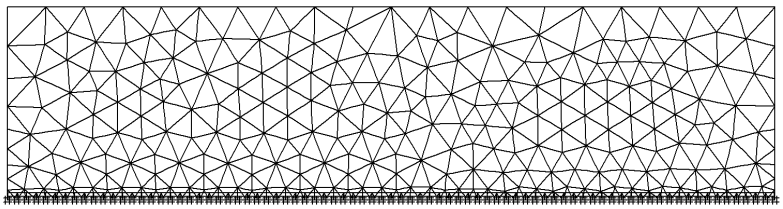

Figure 3.8 Finite element mesh for the sliding block

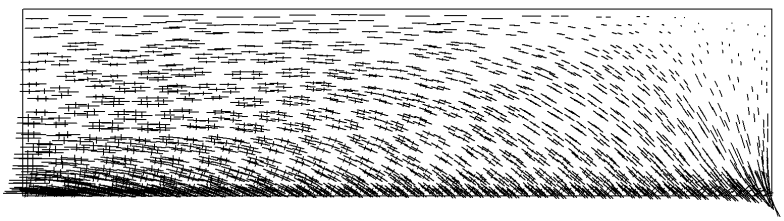

Figure 3.9 Stress distribution

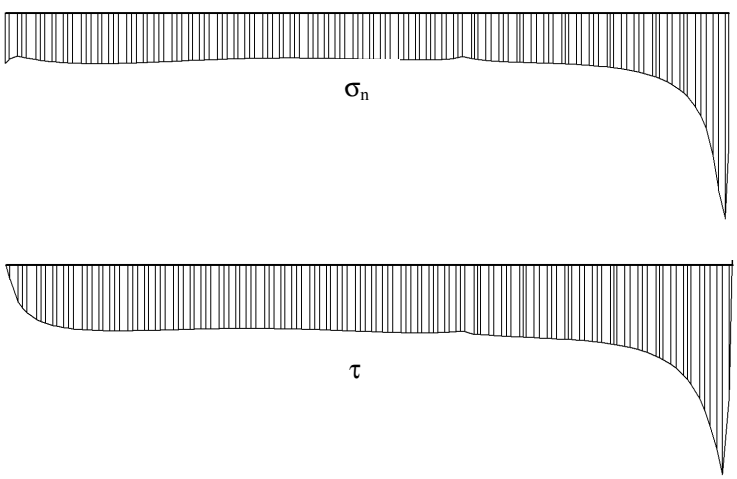

Figure 3.10 Stresses underneath sliding block

Verification: No theoretical solution exists for verifying the internal stress distribution or the distribution of the contact stresses. However, the final sliding force can be calculated as:

$$Failure\ force = width \cdot c_w + weight \cdot \tan \phi_w = 4 \times 2.5 + 100 \times 0.5 = 60 \text{ kN/m}$$

Obviously, the numerical calculation is in good agreement with the theoretical one.

3.4 CYLINDRICAL CAVITY EXPANSION

Expansion of a cylindrical cavity in an elastic perfectly-cohesive soil has been studied by a number of researchers and a theoretical solutions exist for both large and small displacements, Sagaseta (1984). A cylindrical cavity of initial radius a_o is expanded to radius a by the application of an internal pressure p, Figure 3.11. The radius of the elastic-plastic boundary is represented by r. The soil is assumed incompressible with an angle of friction of zero and a cohesion c.

Small displacement solution:

$$r^2 = 2\left(\frac{G}{c}\right)a_o(a - a_o)$$

$$p = \frac{2G(a - a_o)}{a_o} \quad \text{for } r < a_o \qquad p = c - 2c\ \ln\left(\frac{a_o}{r}\right) \quad \text{for } r > a_o$$

Large displacement solution:

$$r^2 = \frac{1}{\eta_r^2}\left(a^2 - a_o^2\right)$$

$$p = GF(\eta) \text{ for } r < a \qquad p = GF(\eta_r) + 2c\ \ln\left(\frac{\eta}{\eta_r}\right) \quad \text{for } r > a$$

where:

$$\eta^2 = \frac{a^2 - a_o^2}{a^2} \qquad \eta_r^2 = 1 - \exp\left(\frac{-c}{G}\right) \qquad F(\eta) = \eta^2 + \frac{\eta^4}{4} + \frac{\eta^6}{9} + \ldots$$

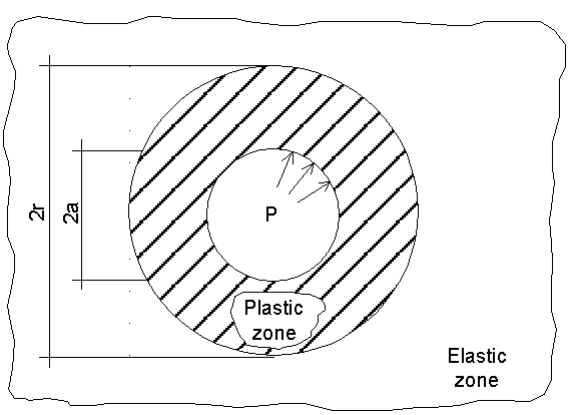

Figure 3.11 Cylindrical cavity expansion

Input: An axisymmetric mesh is used for the calculation of the cylindrical cavity problem, Figure 3.12. In these calculations the ratio G/c is taken to be 100 and Poisson's ratio is 0.495. Since the theoretical solutions are based on an infinite continuum, a

correcting material cluster is added to the perimeter of the mesh. This correcting cluster has a Poisson's ratio of 0.25 and a Young's modulus of $5E/12$ where E is the soil Young's modulus. The quantification of the correcting layer properties is described in Burd & Houlsby (1990). The tension cut-off must be deactivated to get correct results.

Results: The computed relationships between cavity pressure and radial displacement are given in Figure 3.13. It can be seen that the computed results agree very well with the analytical solutions. In order to obtain the cavity pressure from the PLAXIS results it is necessary to divide the computed force per unit radian acting on the cavity surface by the thickness of the soil slice and the cavity radius. The large displacement solution was obtained with an update mesh analysis.

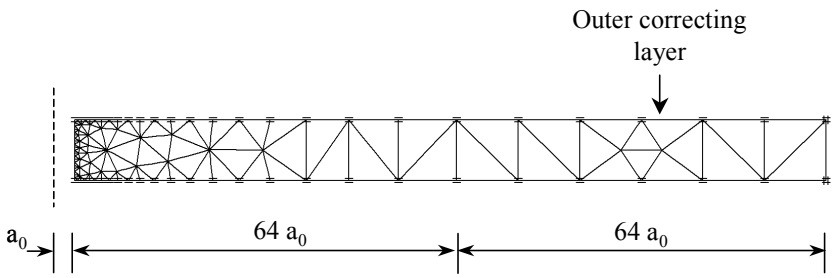

Figure 3.12 Mesh for cavity expansion

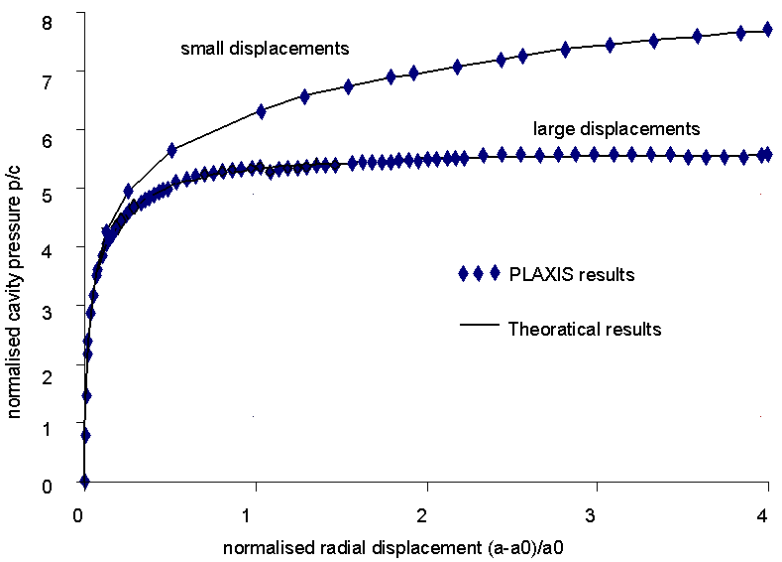

Figure 3.13 Relationships between radial displacement and cavity pressure

4 CONSOLIDATION AND GROUNDWATER FLOW

In this Chapter, some problems involving pore pressure are described. For verification, numerical results computed by PLAXIS are compared with analytical solutions. The first example involves the classical problem of one-dimensional consolidation and the other examples involve groundwater flow problems.

4.1 ONE-DIMENSIONAL CONSOLIDATION

Input: Figure 4.1 shows the finite element mesh for the one-dimensional consolidation problem. The thickness of the layer is 1.0 m. The layer surface (upper side) is allowed to drain while the other sides are kept undrained by imposing closed consolidation boundary condition. It is not necessary to generate initial pore pressures or effective stresses. An excess pore pressure, p_0, is generated by using undrained material behaviour and applying an external load p_0 in the first (plastic) calculation phase. In addition, ten consolidation analyses are performed to ultimate times of 0.1, 0.2, 0.5, 1.0, 2.0, 5.0, 10, 20, 50 and 100 days respectively.

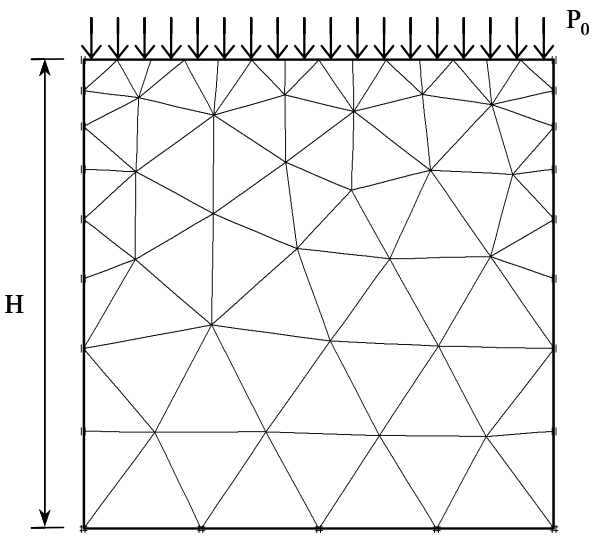

Figure 4.1 Problem geometry and finite element mesh

Output: Figure 4.2 shows the relative excess pore pressure versus the relative vertical position. Each of the above consolidation times is plotted. Figure 4.3 presents the development of the relative excess pore pressure at the (closed) bottom.

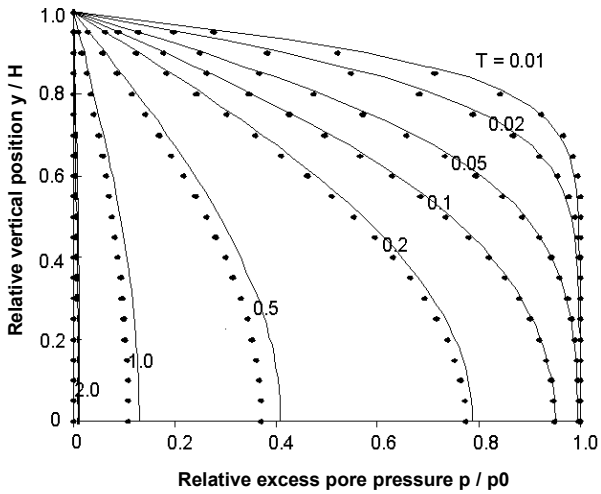

$$T = \frac{c_v t}{H^2}$$

$$c_v = \frac{kE_{oed}}{\gamma_w}$$

$$E_{oed} = \frac{(1\text{-}\nu)E}{(1+\nu)(1\text{-}2\nu)}$$

Figure 4.2 Development of excess pore pressure as a function of the sample height

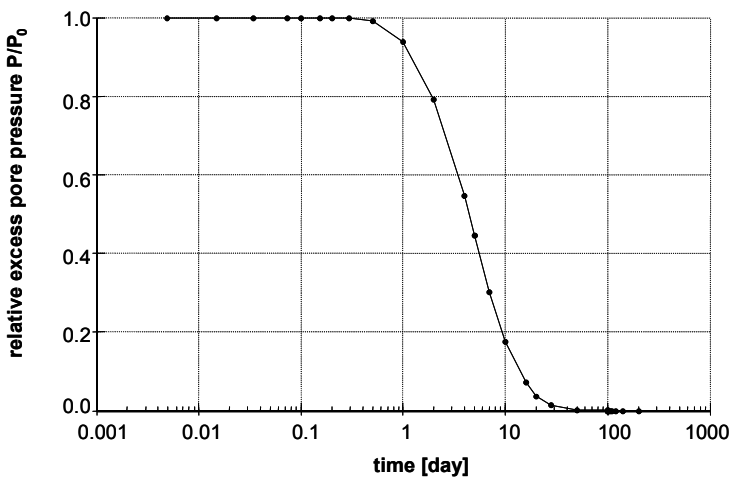

Figure 4.3 Development of excess pore pressure at the bottom of the sample as a function of time

Verification: The problem of one-dimensional consolidation can be described by the following differential equation for the excess pore pressure *p*:

$$\frac{\partial p}{\partial t} = c_v \frac{\partial^2 p}{\partial z^2} \tag{4.1}$$

where:

$$c_v = \frac{kE_{oed}}{\gamma_w} \qquad E_{oed} = \frac{(1-\nu)E}{(1+\nu)(1-2\nu)} \qquad z = H - y \tag{4.2}$$

The analytical solution of this equation, i.e. the relative excess pore pressure, p / p_0 as a function of time and position is presented by Verruijt (1983):

$$\frac{p}{p_0}(z,t) = \frac{4}{\pi} \sum_{j=1}^{\infty} \frac{(-1)^{j-1}}{2j-1} \cos\left((2j\text{-}1)\frac{\pi}{2}\frac{y}{H}\right) \exp\left(-(2j\text{-}1)^2 \frac{\pi^2}{4}\frac{c_v t}{H^2}\right) \tag{4.3}$$

This solution is presented by the dotted lines in Figure 4.2. It can be seen that the numerical solution is close to the analytical solution.

4.2 UNCONFINED FLOW THROUGH A SAND LAYER

This exercise illustrates leakage from a canal into a nearby river through a sand structure.

Input: Figure 4.4 shows the geometry and finite element mesh for the problem. The thickness of the layer is 3.0 m and the length is 10 m. At the right hand side the element distribution is locally refined to a tenth of the global element size. The bottom of the layer is impermeable. On the left hand side the groundwater head is prescribed at 2.0 m and at the right hand side at 1.0 m. The permeability k is 1.0 m/day.

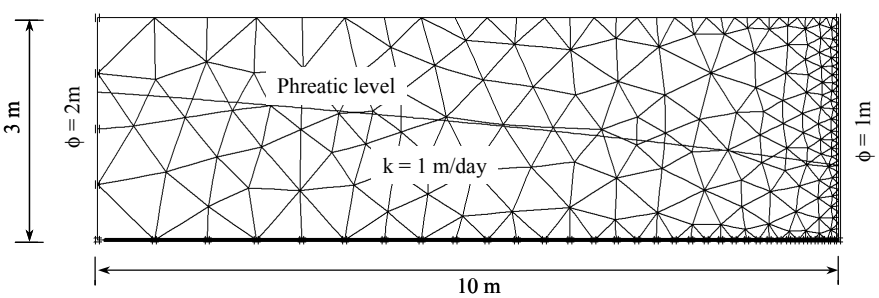

Figure 4.4 Problem geometry and finite element mesh

Output: The steady state solution computed by PLAXIS is presented in Figure 4.5 and Figure 4.6. Figure 4.5 shows the flow field. The computed total discharge is 0.152 m^3/day (per meter in the out of plane direction).

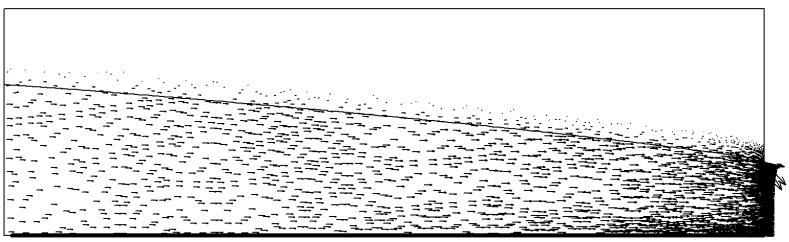

Figure 4.5 Flow field and total discharge Q = 0.152 m^3/day

Figure 4.6 shows the distribution of the groundwater head, going from 2.0 m at the left hand boundary to 1.0 m at the right hand boundary. It can be seen that the contour lines are nearly vertical, which is in agreement with what really happens in such a case. Here, the pore pressure distribution in each vertical cross section is more or less hydrostatic.

If the fall of the groundwater head would be over a smaller length, then the pore pressure distribution would not approximately be hydrostatically, particularly near the right hand boundary.

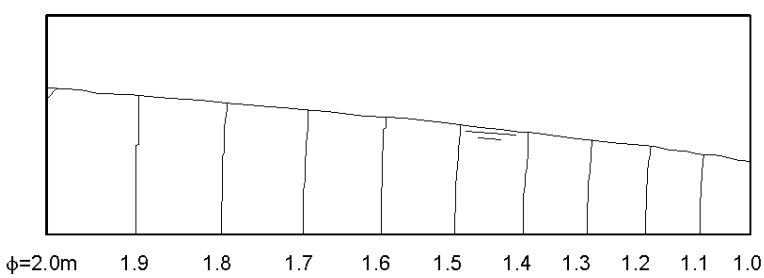

Figure 4.6 Contour lines of groundwater head

Verification: Under the assumption of a hydrostatic pore pressure distribution for each vertical cross section the total discharge through the layer, Q, can be approximated with Dupuis' formula for unconfined flow:

$$Q = k \frac{\varphi_1^2 - \varphi_2^2}{2L} \qquad \text{(per unit of width)} \qquad (4.4)$$

where k is the permeability, L is the length of the layer and ϕ_1 and ϕ_2 are the groundwater head at the left and right boundary respectively. For the current situation this results in a theoretical solution of 0.150 m^3/day/m. The error in the numerical solution is 1.3%.

4.3 CONFINED FLOW AROUND AN IMPERMEABLE WALL

This example illustrates the problem of confined flow around an impermeable wall.

Input: Figure 4.7 shows the geometry and finite element mesh for the problem. The geometry is assumed to consist of a 10 m wide impermeable dam founded on a soil layer of 10.0 m thickness. The bottom of the soil layer is impermeable. A 5.0 m long wall is placed under the dam. At one side of the dam the water level is 5.0 m and at the other side the water level is 3.0 m. The wall is simulated by means of an impermeable interface. (A beam cannot be used here since this type of elements is fully permeable.) The element mesh is locally refined around the wall, in particular at the tip of the wall. The permeability of soil is 1.0 m/day.

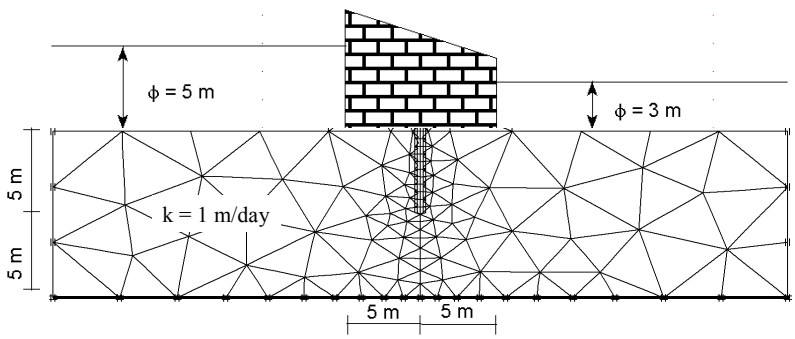

Figure 4.7 Geometry and finite element mesh for flow around a wall

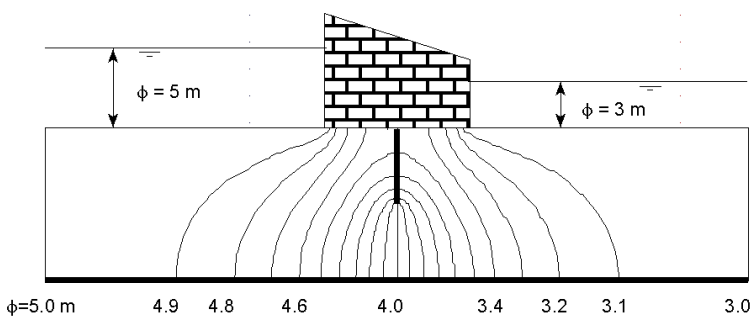

Figure 4.8 Contour lines of groundwater head

Output: The steady state solution computed by PLAXIS is presented in Figure 4.8 and Figure 4.9. The solution is obtained in a single iteration since the flow is confined. Figure 4.8 shows the groundwater head contours, ranging from 5.0 m at the left hand side to 3.0 m at the right hand side. Figure 4.9 shows a detail of the flow field around the wall. The total discharge is 0.818 m^3/day (per meter in the out of plane direction).

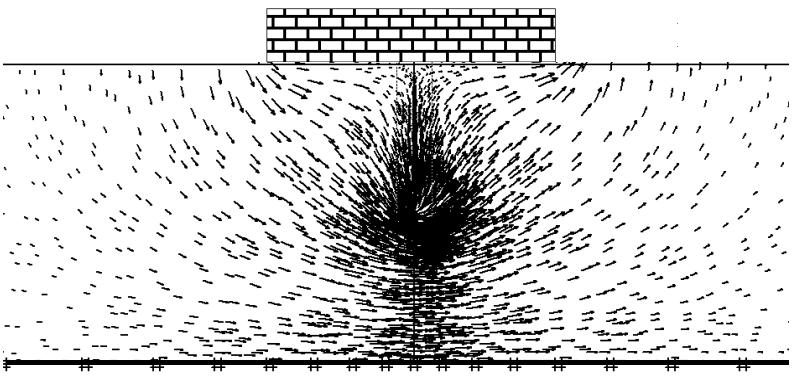

Figure 4.9 Detail of flow field around the wall

Verification: Harr (1962) has given a closed form solution for the discharge of the problem of confined flow around a wall for different geometrical ratios. The solution is presented in Figure 4.10. In the situation described here (s/T=0.5; b/T=0.5) the solution is:

$$Q / k / \Delta h = 0.4$$

which gives a total discharge of 0.8 m^3/day/m. The error in the numerical solution is 2.3%. The solution can be improved by extra refinement of the mesh around the tip of the wall.

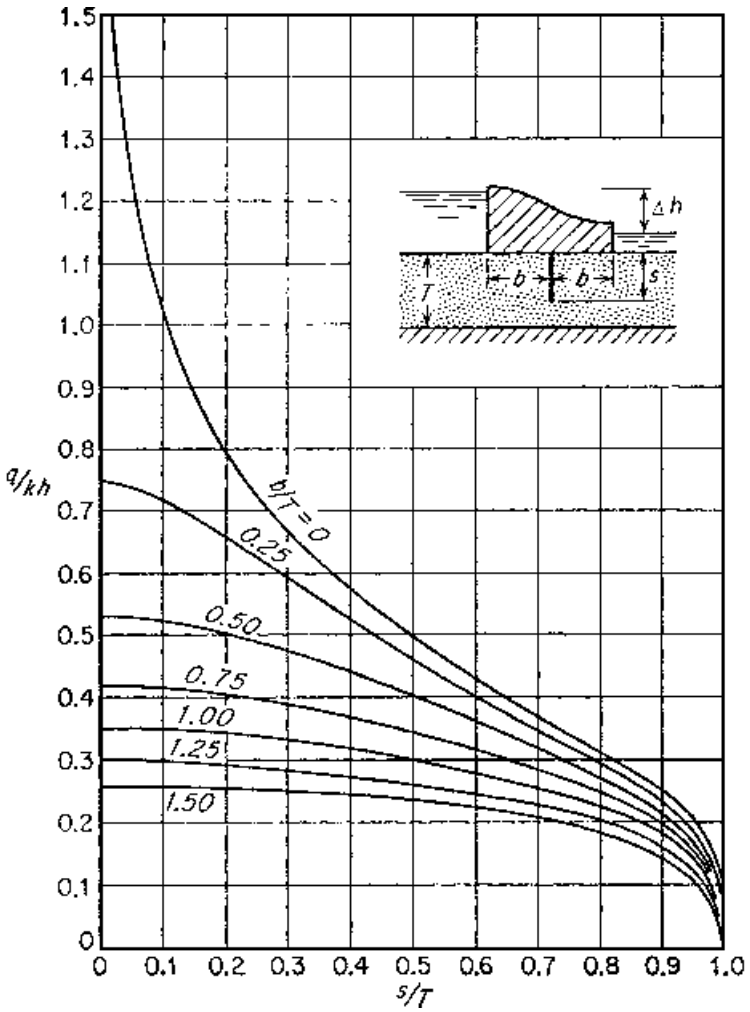

Figure 4.10 (after Harr, 1962)

5 REFERENCES

[1] Blake, A., (1959), Deflection of a Thick Ring in Diametral Compression, Am. Soc. Mech. Eng., J. Appl. Mech., Vol. 26, No. 2.

[2] Burd, H.J. and Houlsby, G.T., (1990), Analysis cylindrical expansion problems. Int. J. Num. Analys. Mech. Geomech. Vol 14, 351-366.

[3] Cox, A.D. (1962), Axially-symmetric plastic deformations - Indentation of ponderable soils. Int. Journal Mech. Science, Vol. 4, 341-380.

[4] Davis, E.H. and Booker J.R., (1973), The effect of increasing strength with depth on the bearing capacity of clays. Geotechnique, Vol. 23, No. 4, 551-563.

[5] Gibson, R.E., (1967), Some results concerning displacements and stresses in a non-homogeneous elastic half-space, Geotechnique, Vol. 17, 58-64.

[6] Giroud, J.P., (1972), Tables pour le calcul des foundations. Vol.1, Dunod, Paris.

[7] Harr, M.E., (1962), Groundwater and seepage. McGraw-Hill. NY

[8] Mattiasson, K., (1981), Numerical results from large deflection beam and frame problems analyzed by means of elliptic integrals. Int. J. Numer. Methods Eng., 17, 145-153.

[9] McMeeking, R.M., and Rice, J.R. (1975). Finite-element formulations for problems of large elastic-plastic deformation. Int. J. Solids Struct., 11, 606-616.

[10] Poulos, H.G. and Davis, E.H., (1974), Elastic solutions for soil and rock mechanics. John Wiley & Sons Inc., New York.

[11] Roark, R. J., (1965), Formulas for Stress and Strain, McGraw-Hill Book Company.

[12] Sagaseta, C., (1984), Personal communication.

[13] Van Langen, H, (1991). Numerical Analysis of Soil-Structure Interaction. PhD thesis Delft University of Technology. Plaxis users can request copies.

[14] Verruijt, A., (1983), Grondmechanica (Geomechanics syllabus). Delft University of Technology.